Polarization effects at the surface of aqueous alkali halide solutions

György Hantal [a],[*], Jiří Kolafa [b], Marcello Sega [c], Pál Jedlovszky [d],[*]

[a] *Institute of Physics and Materials Science, University of Natural Resources and Life Sciences, Peter Jordan Straße 82, A-1190 Vienna, Austria*
[b] *Department of Physical Chemistry, University of Chemistry and Technology, 166 28 Prague 6, Czech Republic*
[c] *Department of Chemical Engineering, University College London, London WC1E 7JE, United Kingdom*
[d] *Department of Chemistry, Eszterházy Károly Catholic University, Leányka utca 6, H-3300 Eger, Hungary*

ABSTRACT

The polarizability of ions, with its strong influence on their surface affinity, is one of the crucial pieces of the complex puzzle that determines the surface properties of electrolyte solutions. Here, we investigate the electrical and structural properties of alkali halide solutions at a concentration of about 1.3 M using molecular dynamics simulations of polarizable water and ions models. We show that capillary fluctuations have a dramatic impact on the sampled quantities and that without removing their smearing effect, it would be impossible to resolve the local structure of the interfacial region. This procedure allows us to investigate in detail the dependence of the permanent and induced dipoles on the distance from the interface. The enhanced resolution gives us access to the surface charges, estimated using the Gouy-Chapman theory, despite the Debye length being shorter than the amplitude of capillary fluctuations.

1. Introduction

The surface structure of alkali halide solutions did not attract considerable scientific interest for almost a century, simply because alkali halides are known to be capillary inactive solutes. Indeed, salts consisting of simple monovalent ions increase the surface tension of water [1–4], indicating, through the Gibbs equation of adsorption [5,6], that they are present at a lower concentration in the vicinity of the surface than in the bulk of their aqueous solutions. Further, salts consisting of multivalent ions are depleted at the surface of their aqueous solutions even more than those of monovalent ions are. This behaviour was explained by Onsager and Samaras almost a century ago using the law of image charges, describing the ions as simple point charges [7].

This view was challenged at the turn of the millennium both by experimental [8–12] and computer simulation [13–17] studies, revealing that large halide ions, in particular, I^{−}, are accumulated at the surface of their aqueous solutions both in droplets [8,9,13–15] and at planar interfaces [10–12,16,17]. This finding, confirmed by numerous subsequent computer simulation [18–29] and density functional theory (DFT) studies [30], was later explained by Levin et al., who extended the theory of Onsager and Samaras to polarizable ions of finite size, and showed that their surface affinity increases both with their polarizability [31] and size [32]. However, despite the observed surface affinity of the

I^{−} ion, alkali iodide salts are still capillary inactive solutes. This seeming contradiction can be resolved considering that, due to the requirement of macroscopic electroneutrality, the surface excess density of cations and anions must be equal [33], and even the largest alkali cation, i.e., Cs^{+}, is far too small to be capillary active. Thus, the effective attraction of the I^{−} ions to and the effective repulsion of its alkali counterions from the liquid surface results in a net negative surface excess [28], and hence to an increase of the surface tension. This view was recently further elaborated by Seki et al., who showed, by performing a combined study of sum frequency generation spectroscopy experiments and computer simulations, that the surface propensity of ions in solutions containing more than one type of ions of the same charge also depends on that of the other ions bearing like charges [34]. From a structural point of view, this behaviour leads, besides the excess concentration of the I^{−} ion at the liquid surface, to its depletion in the subsurface region [18,28]. This explanation suggests that alkali iodide salts are capillary inactive because of the small alkali cation, and if I^{−} would be accompanied by a large enough cation, the salt could be capillary active. In accordance with this view, we have recently showed that tetramethylammonium iodide, consisting of a quasi-simple monovalent cation the size of which is comparable to that of I^{−}, is indeed a capillary active salt [35]. Further, the fictitious salt consisting of the I^{−} anion and a cation that is, apart from the sign of its charge, identical with I^{−}, has also been proven

---

capillary active [36].

Thermal capillary waves play an important role in shaping the surface of the solution, and their effect must be taken into account when investigating the structure of the interface at the molecular scale [37]. For this purpose, the real, capillary wave corrugated, so-called 'intrinsic' surface of the liquid phase has to be identified. Since the pioneering work of Chacón and Tarazona [38], a number of methods aimed at removing the smearing effect of capillary waves have been proposed [39–43], among which the Identification of the Truly Interfacial Molecules (ITIM) [41] turned out to be an excellent compromise between computational cost and accuracy [44]. After identifying the intrinsic liquid surface and the molecules pertaining to the surface layer (and, also, to the subsequent molecular layers), the surface properties of the system can be discussed in terms of profiles calculated relative to the local position of the liquid surface (often referred to as 'intrinsic profiles') as well as in a layer-by-layer manner [45]. Further, it has repeatedly been shown that neglecting the effect of capillary waves, e.g., calculating profiles in the global reference frame (referred to as 'non-intrinsic profiles') blurs the underlying, microscopic structure of the interfacial region [28,41,46–49]. However, despite the wealth of computer simulation studies of the liquid–vapour interface of simple salt solutions and the emergent importance of intrinsic surface analysis in such studies, the surface of aqueous alkali halide solutions has scarcely been studied this way so far [23–29,50].

In a recent set of investigations, we have studied the surface propensity [28] and surface dynamics [29] of alkali chloride and sodium halide salts in aqueous solutions by computer simulations combined with intrinsic surface analysis, considering both non-polarizable and polarizable potential models. We have found that while large anions occur in higher concentration in the surface layer than in the bulk phase, the next 3–4 molecular layers account for their net negative surface excess, because of the effective repulsion of the small cations from the liquid surface [28]. Further, anions stay at the liquid surface for a relatively long time, while cations only visit the surface layer for short times due to thermal fluctuations [29]. Moreover, unlike surface water molecules [51], halide anions do not exhibit enhanced mobility at the liquid surface because they are shielded by the neighbouring water molecules from being exposed to the vapour phase as much as possible [29].

Having analyzed the accumulation and dynamics of alkali halide ions at the surface of their aqueous solution [28,29], here we focus our attention on the interplay between polarization and the proximity to the liquid surface. Considering the widely accepted fact that the polarizability of simple ions increases their surface affinity, it is important to understand how the induced dipole moment of the different particles changes upon going from the bulk liquid phase towards the liquid surface. Here, we investigate these changes in the local polarization upon approaching the liquid surface using molecular dynamics simulations of a polarizable model of water and ions. In particular, we analyze on a per-layer basis (in the first four layers): i) the orientation and magnitude of the induced dipole moment of the ions and water molecules; ii) the orientation of the permanent dipole moment of the water molecules and, iii) the relative orientation of the permanent and induced dipole moments of water. Additionally, we investigate the change of the average magnitude and orientation of the induced dipole moment as a function of the distance from the liquid surface. As we will show, the electric field generated by the addition of salt thanks to the different surface affinities of its cations and anions is compatible with the Gouy-Chapman solution [52], and induces an excess polarization in water that decays exponentially towards the bulk. Given the small surface potentials involved this is, of course, just a perturbation of the main orientation of the water dipoles that, at the surface, keep pointing roughly within the surface plane itself. This is not the case for the polarization of ions, which is directed along the surface normal. Removing the smearing of capillary waves turns out to be the key to access all these quantities.

2. Computational details

The liquid–vapour interface of aqueous alkali chloride (i.e., LiCl, NaCl, KCl, RbCl, CsCl) and sodium halide (i.e., NaF, NaCl, NaBr, NaI) solutions has been simulated in the canonical (N,V,T) ensemble by molecular dynamics at 298 K, using the polarizable AH/BK3 [53] and BK3 [54] models of the ions and water molecules, respectively. The simulations performed have been described in detail in our previous publications [28,29], thus, they are only briefly reminded here.

The simulations have been done using the program MACSIMUS [55]. The rectangular basic simulation box, having the X, Y, and Z edge lengths of 265 Å, 62.818 Å, and 62.818 Å, respectively (X being the interface normal), has consisted of 192 ion pairs and 8000 water molecules. This composition corresponds to the nominal molality of 1.33 m (i.e., the concentration of roughly 1.3 M). The width of the liquid slab is safely (i.e., about an order of magnitude) larger than the Debye screening length, $1/\kappa$, of the ions. The models employed describe the interaction of the particles by the Buckingham potential [56] and Gaussian charge distributions, and account for the polarization using the charge-on-spring method with harmonic springs [53,54]. Dispersion and electrostatic interactions have been cut off beyond 12 Å and 18 Å, respectively. The long range part of the Buckingham potential and the electrostatic interaction has been accounted for using slab cut-off correction and Ewald summation [56–58] with the reciprocal space separation parameter of 0.1953 Å^{-1}, respectively. The Yeh-Berkowitz correction [59] has been applied. Equations-of-motion have been integrated by the Verlet algorithm [56] with the integration time step of 1.67 fs. To keep the water molecules rigid, the SHAKE algorithm [60] has been used. The temperature has been controlled by the Nosé-Hoover thermostat [61,62] with the coupling time of 0.3 ps. Induced dipoles have been integrated by means of the ASPC method [63]. Simulations have been started from configurations pre-equilibrated with a non-polarizable model [28]. After 70 ns equilibration, 10,000 sample configurations, separated by 1 ps long trajectories each, have been dumped for the analyses from the 10 ns long production runs.

For reference purposes, results of similar simulations, performed with the non-polarizable model of ions proposed by Joung and Cheatham [64] (referred to as the JC model) and the SPC/E model of water [65], are also used. These models employ point charges and the Lennard-Jones potential. The simulations with the non-polarizable models have been done with the GROMACS 2019.4 program package [66], using the Nosé-Hoover thermostat with the time constant of 1 ps. All interactions have been truncated to zero beyond 12 Å; their long-range parts have been estimated by the smooth particle mesh Ewald (PME) method [67,68]. The geometry of the water molecules has been kept unchanged using the SETTLE algorithm [69]. The integration time step of 2 fs has been used. Following a 2 ns long equilibration period, 5000 sample configurations have been collected for the analyses from a 20 ns long production run.

The particles forming the first four molecular layers beneath the liquid surface have been identified by the ITIM method [41] using the freely available [70] Pytim software [71]. In the analysis, the grid spacing of the test lines of 0.4 Å and the probe sphere radius of 2 Å have been used, in accordance with previous recommendations [41,44]. The size of the particles, used when deciding whether they are in a touching position with the probe sphere, have been defined through the distance at which the repulsion/dispersion term of their homonuclear interaction becomes zero (see Table 1 of Ref. [28]).

3. Results and discussion

3.1. Orientation of the permanent dipoles of the water molecules

The orientation of the permanent and induced dipole moments of the particles relative to the liquid surface is characterized here by the angles ϕ and ϕ_i, respectively. These angles are formed by the respective (i.e.,

Table 1

Polarizability of the different particles considered [52,53], and average magnitude of the dipole moment induced on them in the bulk liquid phase. The value of $|\mu^{ind}|$ is calculated by averaging the corresponding $\langle|\mu^{ind}|\rangle(X_{intr})$ profiles beyond the X_{intr} value of 9 Å, using the profiles obtained in the alkali chloride solutions for the cations, in the sodium halide solutions for the anions, and in neat water for water.

	Li$^+$	Na$^+$	K$^+$	Rb$^+$	Cs$^+$	F$^-$	Cl$^-$	Br$^-$	I$^-$	water
α/Å^3	0.032	0.157	0.830	1.37	2.36	1.30	3.50	4.60	7.50	0.72[a] 0.36[b]
$|\mu^{ind}|$/mD	0.502	1.79	8.91	13.8	21.4	23.8	57.4	71.4	100	815

[a] Polarizability of the H atoms.

[b] Polarizability of the non-atomic interaction site, located along the bisector of the H—O—H bond angle.

permanent or induced) dipole moments with the surface normal vector, **X**, pointing from the liquid to the vapour phase. The intrinsic and non-intrinsic profiles of the mean value of the cosine of ϕ, $\langle\cos\phi\rangle$, are shown in Fig. 1.a and b, respectively, as obtained in the different sodium halide (top panels) and alkali chloride (bottom panels) solutions. For reference, the results obtained in neat water are also shown. The intrinsic profiles are plotted as a function of the displacement from the capillary wave corrugated, intrinsic liquid surface, X_{intr}. Negative values of X_{intr} correspond to the liquid phase. The non-intrinsic profiles are shown as a function of the position along the macroscopic surface normal axis, X, the zero value of which is corresponding to the middle of the liquid phase.

The intrinsic profiles exhibit a marked minimum at the vicinity (i.e., within 2 Å) of the liquid surface, followed by a clear maximum at -4 Å $< X_{intr} < -2$ Å. This structure, marking an alternating dipolar orientational preference of the water molecules upon going farther from the liquid surface, is characteristic to the profiles obtained in all systems considered, in accordance with previous studies concerning water at hydrophobic surfaces [72,73]. It is also remarkable that the $\langle\cos\phi\rangle(X_{intr})$ profile does not show any considerable dependence on the type of the cations, while it is shifted to increasingly larger values with increasing anion size in the X_{intr} range between 0 Å and about -6 Å. This shift evidences a tendency of the water molecules to turn their dipoles more to the vapour phase in the presence of sodium halides, in particular, when the halide ion is large, than in their absence. These results are understandable, considering that (i) alkali cations (as well as the Cl$^-$ anion) are strongly depleted from the liquid surface, and hence

the surface region of aqueous alkali chloride solutions is similar to that of neat water, while (ii) the concentration of the halide anions in the surface layer increases with their size, and the excess negative charge imposed at the liquid surface by their presence in enhanced concentration is compensated by the Na$^+$ ions present in the subsequent molecular layers [28]. This charge separation induces a small electric field in the surface region, which affects the dipolar orientation of the surface water molecules. Very similar results have been obtained with the non-polarizable JC and SPC/E models of the ions and water molecules, respectively (see the inset of Fig. 1.a).

It is quite remarkable how much this interfacial structure of the dipolar orientation of the water molecules is blurred by the capillary waves. Thus, the non-intrinsic profiles exhibit a much smoother, less structured wave of considerably smaller amplitude, which damps to zero in a much broader distance range than the corresponding wave of the intrinsic profiles (Fig. 1.b). Further, the maximum, clearly seen in all intrinsic profiles, is even completely washed away by the smearing effect of the capillary waves in certain systems (e.g., in neat water or in the solution of NaF). Moreover, the non-intrinsic profiles are affected by rapidly increasing numerical errors upon approaching the vapour phase due to the progressively decreasing number of particles. On the other hand, this problem does not affect the intrinsic profiles, as the zero value of X_{intr} is set, by definition, by the surface molecules [48].

To further analyze the orientation of the permanent water dipoles at the liquid surface, we have calculated the distribution of $\cos\phi$ at various displacements from the intrinsic liquid surface. The bivariate $P(X_{intr},\cos\phi)$ distributions are shown in Fig. 2 as obtained in neat water and in the
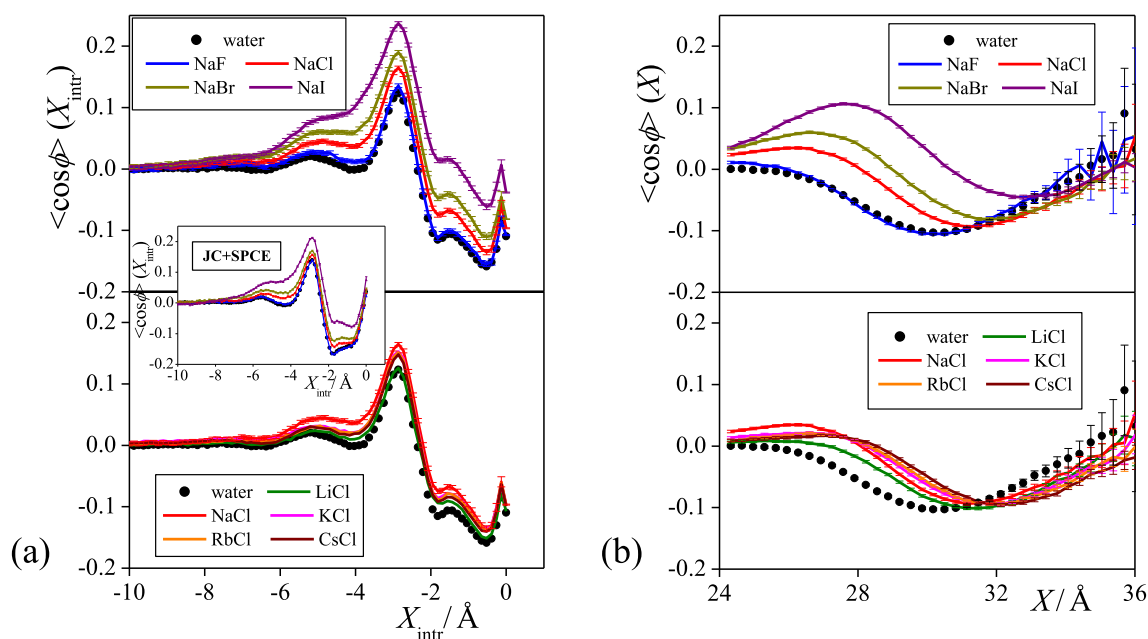

Fig. 1. (a) Intrinsic, and (b) non-intrinsic profiles of the mean value of cos ϕ, as obtained in the sodium halide (top panels) and alkali chloride (bottom panels) solutions simulated (lines). For reference, the profile obtained in neat liquid water is also shown (full circles). The inset shows the intrinsic profiles obtained in sodium halide solutions with the non-polarizable JC and SPC/E models of the ions and water molecules, respectively. The error bars represent standard errors. For the definition of angle ϕ, see the text.
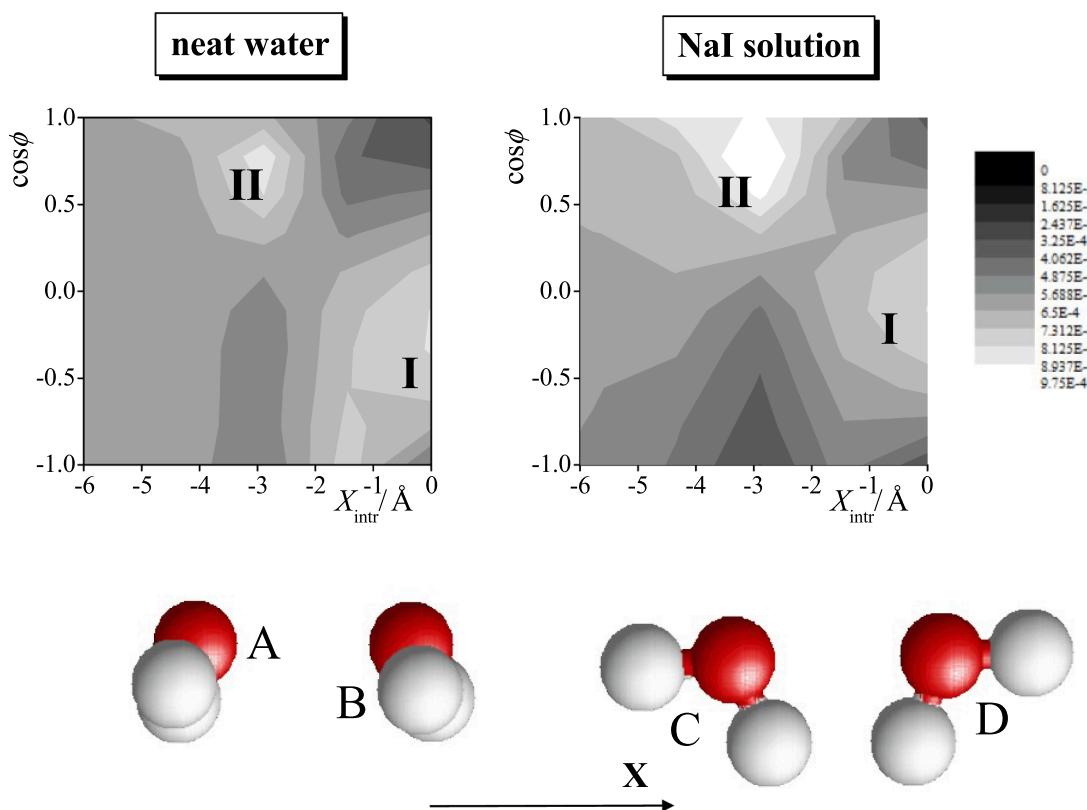
neat water

NaI solution

Fig. 2. Bivariate distribution of the displacement from the intrinsic liquid surface, X_{intr}, and cos ϕ, as obtained in neat water (left) and in the NaI solution (right). Lighter colours correspond to higher probabilities (see the greyscale at the right). The two peaks of the distributions are marked as I and II (see the text). The four preferred orientations of the water molecules at the liquid surface [73] are illustrated at the bottom of the figure. For the definition of angle ϕ, see the text.

NaI solution. As is seen, the bivariate distribution obtained in neat water exhibits two clear peaks, one at $X_{intr} = 0$ Å and cos $\phi \approx -0.2$, and another one at the X_{intr} and cos ϕ values of about –3 Å and 0.7, respectively. These peaks are referred to here as I and II, respectively. The position of these peaks is consistent with our earlier results, concerning the orientational distribution of BK-type polarizable water molecules at the liquid surface [74]. In that study, we found two stronger and two somewhat less strong orientational preferences of the surface water molecules (shown also in Fig. 2) [74]. In the orientations corresponding to the two major preferences, the two O—H bonds form the same angle with the surface normal vector, **X**, (i.e., the water molecule is symmetrically tilted from the macroscopic plane of the surface). In one of these orientations the molecular plane is tilted to the liquid, while in the other one to the vapour phase by the H atoms. These orientations are marked here by A and B, respectively. In the other two, somewhat less strong preferences, one of the two O—H bonds stays parallel with **X**, pointing towards either the liquid or the vapour phase by the H atom (marked by C and D, respectively, see Fig. 2). Orientations A and D prevail at the surface portions of locally convex curvature ('crests'), while B and C at those of locally concave curvature ('troughs') [74]. The present results show that, within the first layer, orientations A and C occur, on average, closer to the intrinsic liquid surface, while B and D occur somewhat farther from it. In the presence of NaI, the preference marked by peak I becomes somewhat weaker, while that marked by peak II gets stronger due to the electric field induced by the different surface affinities of the Na$^+$ and I$^-$ ions, resulting thus in the observed upshift of the $\langle$cos $\phi\rangle(X_{intr})$ profile.

Earlier results showed that, at least in neat water, the presence of the liquid surface only affects the orientation of the molecules pertaining to the surface molecular layer [41,46,47,74]. To investigate this point, we have calculated the $P(\cos \phi)$ distribution in the first four subsurface

molecular layers of neat water and the NaI solution. The results, shown in Fig. 3, reveal that while in the surface layer of water the permanent dipoles prefer to lie more or less parallel with the macroscopic plane of the surface, from the second layer on their orientation is no longer correlated with the liquid surface, as the corresponding $P(\cos \phi)$ distributions are almost uniform. In the presence of NaI, the aforementioned electric field shifts the distribution of the first layer molecules to larger cos ϕ values (i.e., turns the orientation of the dipoles slightly toward the vapour phase). From the second layer on the distributions are of linear shape, with larger probabilities at larger cos ϕ values, and their slope decreases upon going farther from the liquid surface. This finding clearly
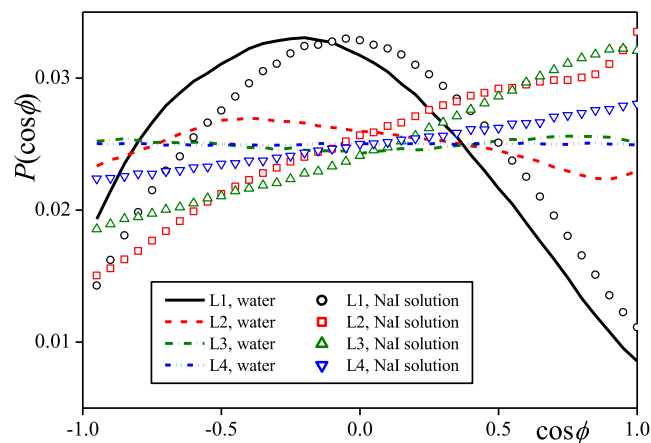

Fig. 3. Distribution of cos ϕ, as obtained in the first (black), second (red), third (green), and fourth (blue) subsurface molecular layer of neat water (lines) and the NaI solution (open symbols). For the definition of angle ϕ, see the text.

suggests that the effect of this electric field is the only factor that correlates the orientation of the water dipoles with the surface in the NaI solution from the second layer on.

3.2. Orientation of the induced dipoles

The intrinsic profiles of the average cosine value of the angle ϕ_i, formed by the induced dipole vector of the particles with the vector **X**, is shown in Fig. 4.a and b, as obtained in the sodium halide and alkali chloride solutions, respectively. Note that the induced dipole (vector) equals the total dipole moment calculated from the actual positions of the Drude charges minus the permanent dipole moment calculated for a molecule in zero electric field. For reference, results obtained in neat water are also reported. Further, the distribution of cos ϕ_i in the first four subsurface layers of the NaCl solution is plotted in Fig. 5 as obtained for the water molecules as well as for the Na$^+$ and Cl$^-$ ions.

The results concerning the induced dipole moment of the water molecules are very similar to those obtained for their permanent dipoles (see Figs. 1 and 3). Thus, the $\langle \cos \phi_i \rangle (X_{intr})$ profiles are again exhibiting the subsequent minima and maxima, and the structured part of the profile is shifted to larger values in the presence of larger halide ions. Further, as in the case of the permanent dipole moments, the distribution of cos ϕ_i is almost uniform from the second layer on (see the top panel of Fig. 5). This strong similarity between the orientational profiles and layer-wise distributions of the induced and permanent dipoles suggests that they likely prefer to stay parallel with each other. To confirm this claim, we have calculated the cosine distribution of the angle γ, formed by the induced and permanent dipoles of the water molecules in the first four layers of neat water and the NaI solution. The obtained distributions, plotted in Fig. 6, indeed show a very strong

preference of the two dipoles for the parallel alignment with each other. This preference is slightly weaker in the NaI solution and in the first layer than in neat water and in the subsequent subsurface layers, respectively. Nevertheless, the integration of these distributions reveal that the angle γ is less than 15° for 40 %, and less than 30° for about 90 % of the water molecules in every case.

The $\langle \cos \phi_i \rangle (X_{intr})$ profiles of the cations, similarly to those of the water molecules, also exhibit a wavy structure within about 4 Å from the intrinsic liquid surface (see Fig. 4). However, in this case, practically the entire structured part of the profile is above zero, indicating the preference of the induced dipoles of the cations to point towards the vapour rather than the liquid phase. This preference is even stronger for the anions, the $\langle \cos \phi_i \rangle (X_{intr})$ profiles of which do not even exhibit the usual wave of a subsequent minima and maxima, but increase steadily with decreasing X_{intr} values, i.e., upon approaching the intrinsic liquid surface, in its vicinity of about 2 Å. The $P(\cos \phi_i)$ distributions of both type of ions are shown in the lower panels of Fig. 5, as obtained in the first four subsurface layers of the NaCl solution. As is seen, while the $P(\cos \phi_i)$ distributions obtained in the first layer exhibit monotonous increase with cos ϕ_i, indicating the preference of the induced dipoles to point straight out to the vapour phase (this preference being considerably stronger for the anions than for the cations), they are again essentially uniform from the second layer on in both cases. (Note also the rather large noise of the distribution corresponding to the cation dipole moments in the first intrinsic layer, caused by the fact that there are only a few cations there.).

3.3. Magnitude of the induced dipoles

In analysing the magnitude of the dipole moments induced on the
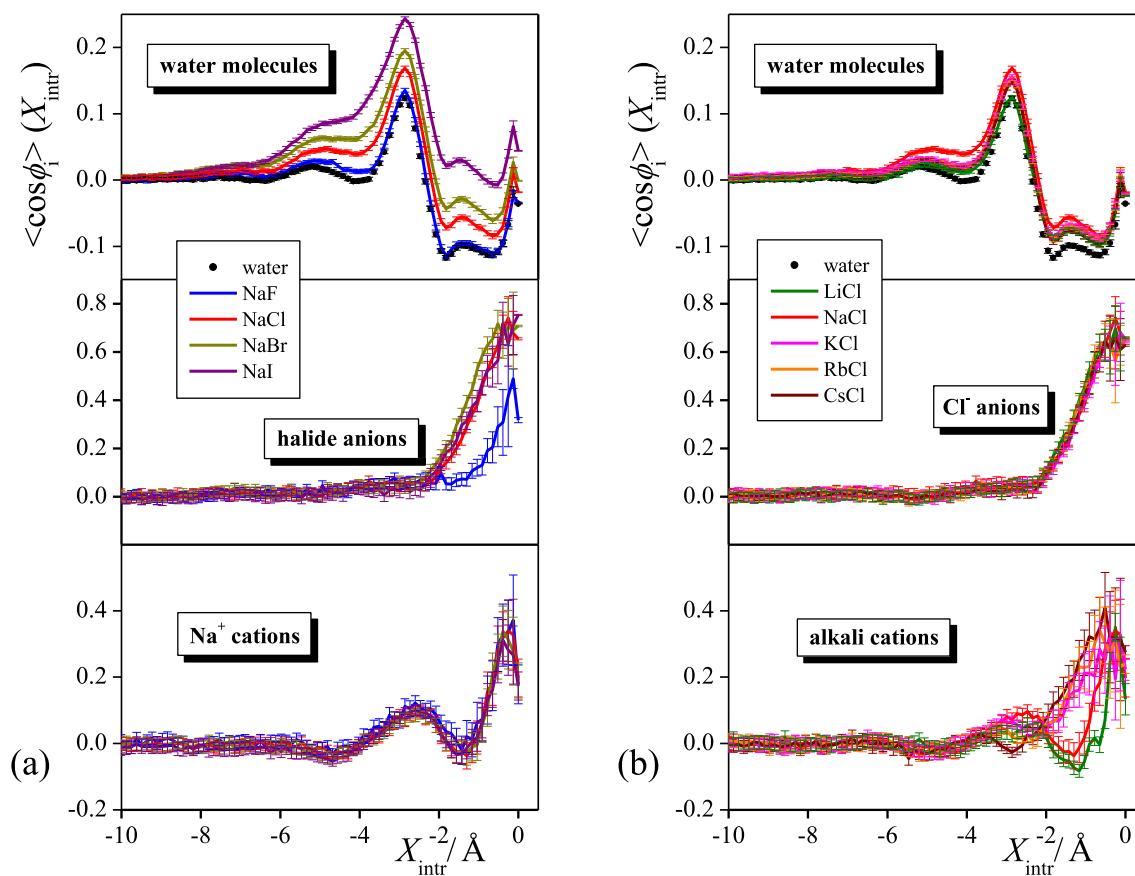

Fig. 4. Intrinsic profiles of the mean value of cos ϕ_i, as obtained (a) in the sodium halide, and (b) in the alkali chloride solutions simulated (lines) for the water molecules (top panels), anions (middle panels), and cations (bottom panels). For reference, the profile obtained for the water molecules in neat liquid water is also shown (full circles). The error bars represent standard errors. For the definition of angle ϕ_i, see the text.
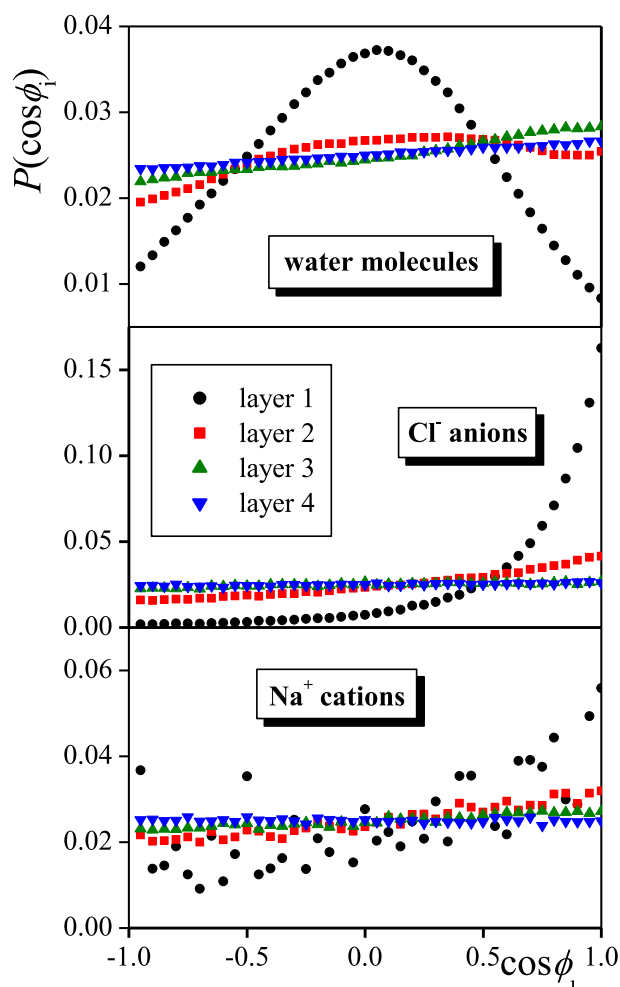
Fig. 5. Distribution of cos ϕ_i, as obtained in the first (black circles), second (red squares), third (green up triangles), and fourth (blue down triangles) subsurface molecular layer of the NaCl solution for the water molecules (top), chloride anions (middle), and sodium cations (bottom). For the definition of angle ϕ_i, see the text.
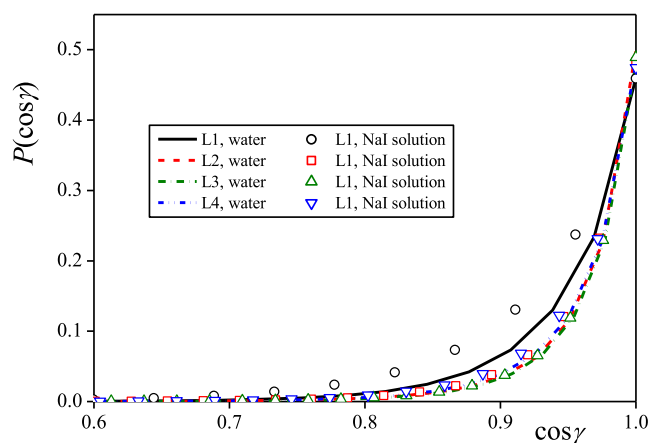

Fig. 6. Distribution of the cosine of angle γ, formed by the permanent and induced dipole moments of the water molecules, as obtained in the first (black), second (red), third (green), and fourth (blue) subsurface molecular layer of neat water (lines) and NaI solution (symbols).
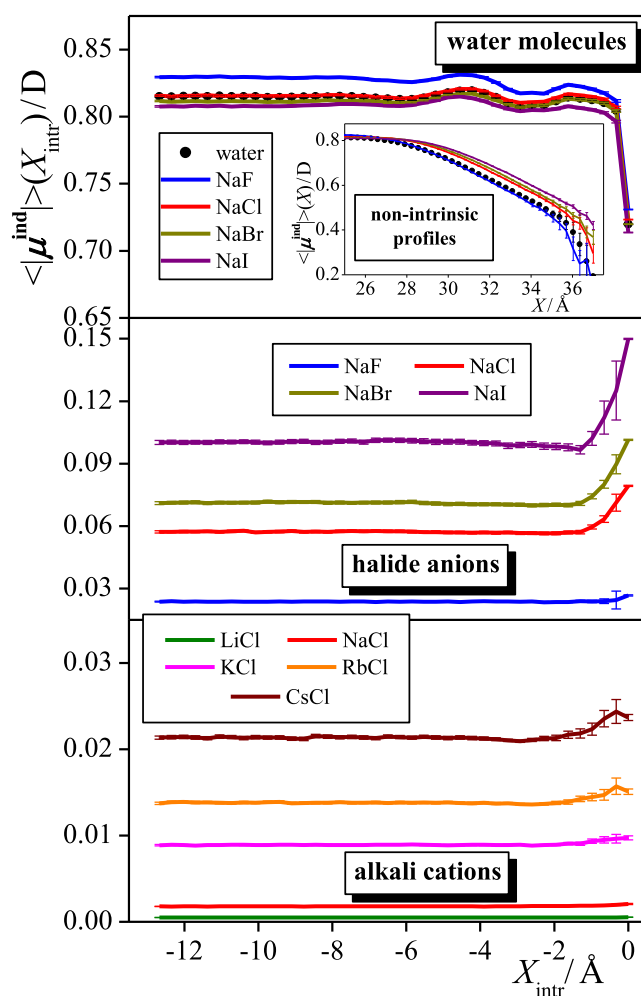

Fig. 7. Intrinsic profiles of the average magnitude of the induced dipole moments of the water molecules (top panels), anions (middle panels), and cations (bottom panels), as obtained in the sodium halide (for water and anions) and alkali chloride (for cations) solutions simulated (lines). For reference, the profile obtained for the water molecules in neat liquid water is also shown (full circles). The inset shows the non-intrinsic profiles of the water molecules obtained in sodium halide solutions. The error bars represent standard errors.

different particles, it has to be emphasized that since the ions bear non-zero net charges, the magnitude of their (induced) dipole moment depends on the choice of the origin. Here, we consider the position of the ion as the origin for this purpose.

The intrinsic profile of the average magnitude of the induced dipole moment, $\langle|\mu^{ind}|\rangle$, of the water molecules and halide anions in different systems are shown in Fig. 7. It should be noted that the magnitude of μ^{ind} of the water molecules does not depend noticeably on the composition of the system. Similar results are obtained for the Na^+ and Cl^- ions, as the magnitude of the dipole moment induced on them also turns out to be practically independent from the type of their counterion. Further, the $\langle|\mu^{ind}|\rangle(X_{intr})$ profiles are always practically constant, apart from their portion very close (i.e., within 1–2 Å) to the intrinsic liquid surface. This means that interface-induced polarization is limited to an 1–2 Å wide layer beneath the liquid surface. In other words, practically only those particles are affected by the vicinity of the interface in this respect that stay (almost) right at the boundary of the two phases, and hence being largely exposed to the vapour phase. The magnitude of the dipole moment induced on the different ions is largely determined by their polarizability, α, as demonstrated by Table 1, collecting the values of the polarizability and average magnitude of the induced dipole moment in the bulk liquid phase for all species considered. As is seen, the ratio of

$\langle|\boldsymbol{\mu}^{\text{ind}}|\rangle$ and α falls between about 9 mD/Å³ and 20 mD/Å³ for all ions, being somewhat smaller for ions of larger size. On the other hand, this value is two orders of magnitude larger for the water molecules.

At the liquid surface, the dipole moment induced on the water molecules is somewhat (i.e., about 10 %) smaller, while those induced on the ions is larger than in the bulk liquid phase. This increase is 10–15 % for the cations, and 10–50 % for the anions, being larger for larger anions. It is again quite striking how much this very sharp change of the intrinsic $\langle|\boldsymbol{\mu}^{\text{ind}}|\rangle(X_{\text{intr}})$ profiles is smeared if the capillary waves are not removed for the analysis. This is illustrated in the inset of Fig. 7, showing the non-intrinsic profile of $\langle|\boldsymbol{\mu}^{\text{ind}}|\rangle$ for the water molecules in the same systems as the intrinsic ones. Thus, while in the case of the intrinsic profile $\langle|\boldsymbol{\mu}^{\text{ind}}|\rangle$ reaches its bulk phase value within 1 Å from the liquid surface, this rise covers an about 8 Å wide interval once the smearing

effect of the capillary waves is not removed.

The distribution of the magnitude of the induced and total dipole moments ($|\boldsymbol{\mu}^{\text{ind}}|$ and $|\boldsymbol{\mu}|$, respectively) of the water molecules in the first four molecular layers of neat water and the NaI solution are shown in Fig. 8.a. Further, the P($|\boldsymbol{\mu}^{\text{ind}}|$) distributions of the halide anions in the first four layers of the sodium halide solutions and those of the alkali cations in the first four layers of the alkali chloride solutions are shown in Fig. 8.b and c, respectively. As is seen, the distributions of the induced and total dipole moments of the water molecules are very similar to each other in every case, apart from an about 1.8 D shift. This result is in full accordance with our above finding that the induced and permanent dipoles of the water molecules strongly prefer to stay parallel with each other (see Fig. 6), considering also that the permanent dipole moment of BK3 water is 1.855 D [54]. It is also seen, in accordance with the
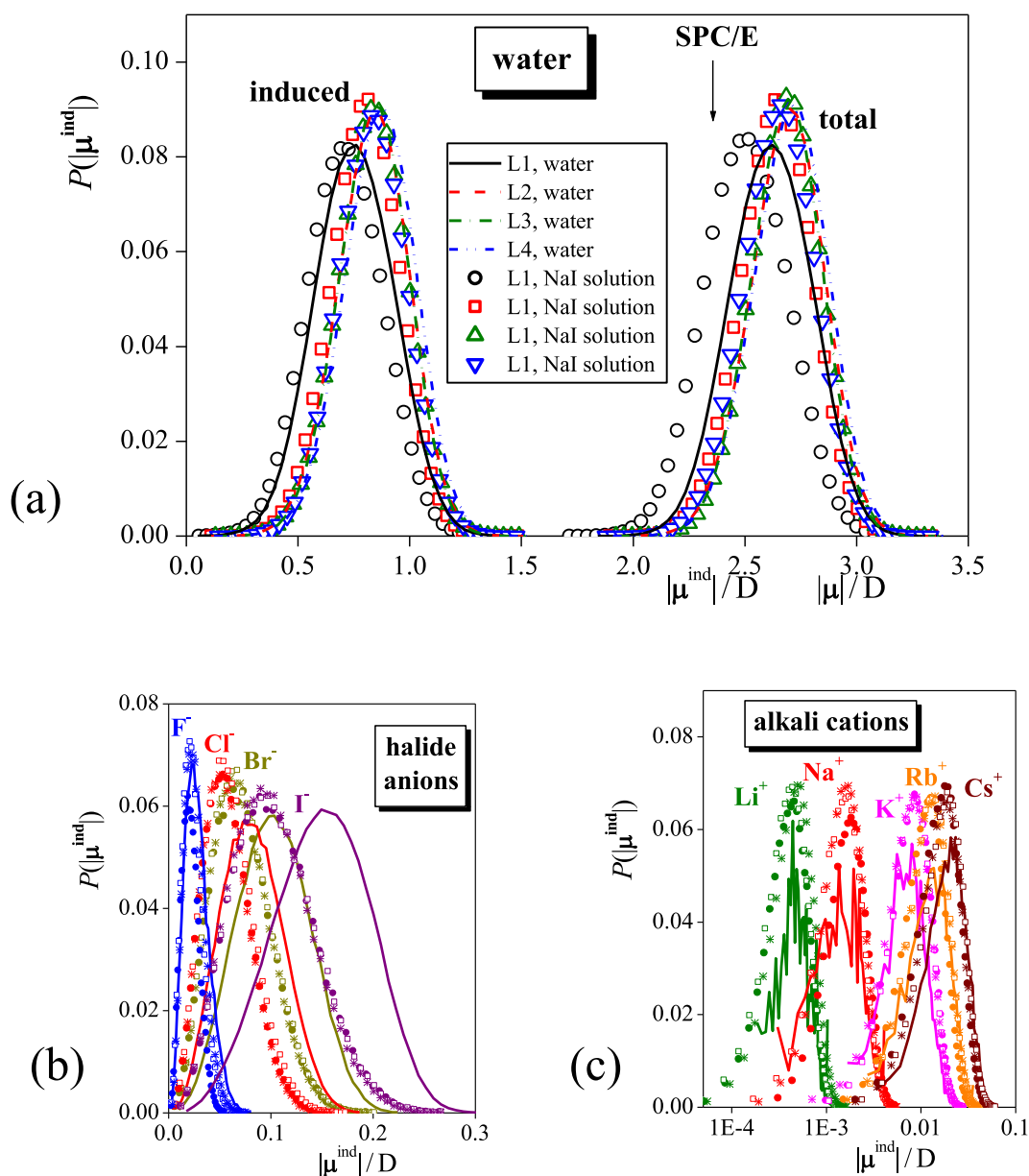

Fig. 8. (a) Distribution of the magnitude of the induced (left) and total (right) dipole moments of the water molecules, as obtained in the first (black), second (red), third (green), and fourth (blue) subsurface molecular layer of neat water (lines) and the NaI solution (open symbols). The arrow marks the dipole moment value of the non-polarizable SPC/E water model. (b) Distribution of the magnitude of the induced dipole moments of the F⁻ (blue), Cl⁻ (red), Br⁻ (khaki), and I⁻ (purple) anions, as obtained in the first (lines), second (filled circles), third (open squares), and fourth (asterisks) subsurface molecular layer of the sodium halide solutions. (c) Distribution of the magnitude of the induced dipole moments of the Li⁺ (green), Na⁺ (red), K⁺ (magenta), Rb⁺ (orange), and Cs⁺ (brown) cations, as obtained in the first (lines), second (filled circles), third (open squares), and fourth (asterisks) subsurface molecular layer of the alkali chloride solutions.

intrinsic profiles of $\langle|\boldsymbol{\mu}^{ind}|\rangle$ (Fig. 7) that the distributions are slightly (i. e., about 0.1 D) shifted to smaller values in the first molecular layer with respect to those in the subsequent ones. An opposite shift of the P($|\boldsymbol{\mu}^{ind}|$) distributions is seen in the first layer for the anions, getting larger with increasing anion size, while it is hard to see any such shift for the cations, as their P($|\boldsymbol{\mu}^{ind}|$) distribution in the first layer is always affected by a very large statistical noise due to their strong depletion at the liquid surface [28]. Nevertheless, it is clear from Fig. 8 that, similarly to the water molecules, the P($|\boldsymbol{\mu}^{ind}|$) distributions of the ions remain essentially unchanged from the second subsurface layer on, in accordance with the behaviour of the corresponding intrinsic profiles (Fig. 7).

3.4. Estimating the effective surface charge density in sodium halide solutions

The high spatial resolution obtained by removing the capillary wave smearing allows us to access the intrinsic profile of the local electric polarization $p(X_{intr})$ of water in the thin interfacial region. We compute p by adding the contributions coming from the permanent and induced dipoles of the water molecules, i.e., $\mu\langle\cos\phi\rangle/v$ and $\langle|\boldsymbol{\mu}^{ind}|\rangle\langle\cos\phi_i\rangle/v$, respectively, where $v = 27$ Å^3 is the volume of the water molecule. The difference between the polarization in the electrolyte solutions and neat water, divided by the electric susceptibility of water, $\chi = (\varepsilon - 1)/4\pi$ (Gaussian units), provides the excess electric field,

$$|\boldsymbol{E}^{exc}|(X_{intr}) = p(X_{intr})/\chi \qquad (1)$$

generated by the ions.

In Fig. 9, we report $|\boldsymbol{E}^{exc}|(X_{intr})$ on a semi-logarithmic scale, showing that it decays exponentially, following the approximation of the Gouy-Chapman solution for small surface potentials [75],

$$|\boldsymbol{E}|(X) = \kappa\psi_0 e^{-\kappa X} \qquad (2)$$

where ψ_0 is the surface potential,

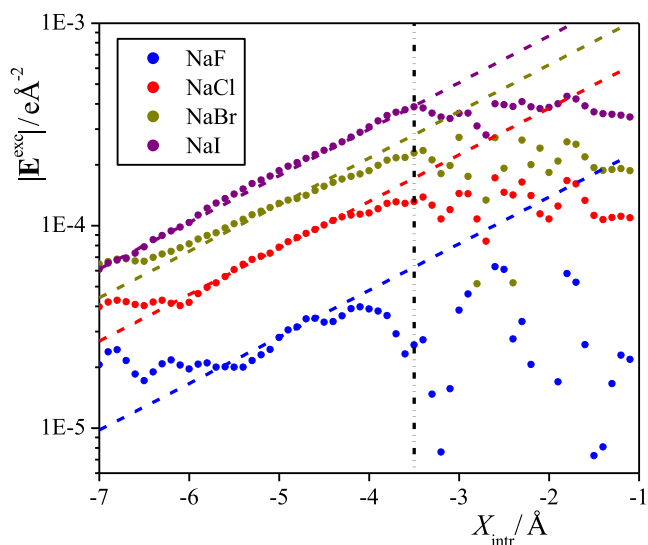$$\kappa = \sqrt{\frac{8\pi e^2 c}{\varepsilon k_B T}} \qquad (3)$$

Fig. 9. Intrinsic profiles of the magnitude of the excess electric field (with respect to neat water), as obtained in the solutions of NaF (blue symbols), NaCl (red symbols), NaBr (khaki symbols) and NaI (purple symbols). To emphasize the exponential decay of these profiles, the results are shown on a logarithmic scale. The exponential functions fitted to the decaying part of the data are shown by straight lines of respective colours. The black vertical dash-dot-dotted line marks the boundary of the electric double layer, beyond which the electric field is constant.

($1/\kappa$ being the Debye length), c is the concentration of the ions, k_B is the Boltzmann constant, and ε is the relative permittivity of water. Here, for simplicity, we disregard the static and dynamic contributions of the ions to the permittivity [76,77]. The results reported in Fig. 9 clearly show the presence of an electric double-layer, where the electric field is constant. This defines the location of the Helmholtz surface at about 3.5 Å from the intrinsic liquid surface. A fit to the exponentially decaying part of the $|\boldsymbol{E}^{exc}|(X_{intr})$ functions allows us to compute the effective surface charge density of the systems, using the electric field at the Helmholtz surface. The obtained values, collected in Table 2, fall in the range of $10^{-4} – 10^{-3}$ e/Å^2, being an order of magnitude larger for NaI than for NaF. These rather small values of the effective surface charge density can, in accordance with the orientational preferences seen, perturb the surface orientation of the water molecules, but by no means can dominate them.

4. Summary and conclusions

In this paper, we have analysed the properties of the induced and permanent dipole moments in aqueous alkali halide solutions, focusing on their dependence on the distance from the (capillary-wave corrugated) liquid surface and on the size of the ions. Removing the smearing effect of capillary waves has turned out to be the key to resolve the alternating structure of maxima and minima in the profile of the dipole orientations and gain access to various quantities. In the presence of large halide anions, in particular, I$^-$, that adsorb at the liquid surface, the structured part of the water orientational profiles is shifted to larger cosine values, indicating a slight turn of the dipole vectors towards the vapour phase. This turn is related to the presence of a small electric field, resulting from the different surface affinities of the large halide anions and small alkali cations. It has also been found that the effect of this electric field is the only factor that correlates the dipolar orientation with the surface from the second layer on. We have interpreted the excess polarization (with respect to the neat water case) in terms of the Gouy-Chapman theory, which has allowed us to estimate the surface charge of the solutions. In addition, we have found large similarities in the behaviour of the induced and permanent dipoles of the water molecules, which can simply be explained by their very strong preference for parallel alignment with each other.

The orientation of the induced dipoles of the ions shows a rather different picture. Thus, while the dipole vector of the water molecules lies preferentially parallel with the macroscopic plane of the surface (the effect of the surface charge being only a perturbation), the dipoles induced on the ions stay preferentially perpendicular to it, pointing towards the vapour phase. Correspondingly, while the magnitude of the dipole moment induced on the water molecules is smaller, that on the ions is larger at the close vicinity of the liquid surface than in the bulk liquid phase. The ratio of the average magnitude of the induced dipole moment and polarizability decreases with increasing ion size. Similarly to their orientation, the magnitude of the induced dipoles differs from the bulk phase value only in the first molecular layer beneath the liquid surface. In other words, polarization effect caused by the interface affects only a 1–2 Å wide region beneath the liquid surface.

Finally, the present results stress the importance of removing the smearing effect of the capillary waves, i.e., the use of intrinsic rather than non-intrinsic profiles in such analyses. Clearly, the very sharp change of the orientation and magnitude of the induced dipoles upon approaching the liquid surface is strongly blurred by the capillary waves (and this blurring would keep slowly increasing with the size of the

Table 2
Effective surface charge density (in e/Å^2 units) obtained in the sodium halide solutions simulated.

NaF	NaCl	NBr	NaI
0.21×10^{-3}	0.58×10^{-3}	0.95×10^{-3}	1.32×10^{-3}

simulated system). Thus, the changes occurring in a distance range of 2–4 Å, always involving almost exclusively the first molecular layer, are smeared in an about 10 Å-wide range by the capillary waves.

CRediT authorship contribution statement

György Hantal: Conceptualization, Methodology, Investigation, Data curation, Formal analysis. **Jiří Kolafa:** Methodology, Software, Investigation. **Marcello Sega:** Data curation, Formal analysis, Investigation, Writing – original draft. **Pál Jedlovszky:** Conceptualization, Funding acquisition, Data curation, Project administration, Resources, Writing – original draft, Writing – review & editing.

Declaration of Competing Interest

The authors declare that they have no known competing financial interests or personal relationships that could have appeared to influence the work reported in this paper.

Data availability

Data will be made available on request.

Acknowledgements

References

[1] A. Heydweiller, About physical properties of solutions in their context. II. Surface tension and electrical conductivity of aqueous salt solutions, Ann. Physik 338 (1910) 145–185, in German.
[2] P.K. Weissenborn, R.J. Pugh, Surface tension of aqueous solutions of electrolytes: Relationship with ion hydration, oxygen solubility, and bubble coalescence, J. Coll. Interface Sci. 184 (1996) 550–563.
[3] K. Ali, A. Haq, S. Bilal, S. Siddiqi, Concentration and temperature dependence of surface parameters of some aqueous salt solutions, Coll. Surf. A 272 (2006) 105–110.
[4] H. Chen, Z. Li, F. Wang, Z. Wang, H. Li, Investigation of surface properties for electrolyte solutions: Measurement and prediction of surface tension for aqueous concentrated electrolyte solutions, J. Chem. Eng. Data 62 (2017) 3783–3792.
[5] D.J. Shaw, Introduction to colloid and surface chemistry, Butterworths, London, 1980.
[6] P. Atkins, J. de Paula, Physical chemistry, Freeman, New York, 2006.
[7] L. Onsager, N.N.T. Samaras, The surface tension of Debeye-Hückel electrolytes, J. Chem. Phys. 2 (1934) 528–536.
[8] G. Markovich, R. Giniger, M. Levin, O. Cheshnovsky, Photoelectron spectroscopy of iodine anion solvated in water clusters, J. Chem. Phys. 95 (1991) 9416–9419.
[9] G. Markovich, S. Pollack, R. Giniger, O. Cheshnovsky, Photoelectron spectroscopy of Cl⁻, Br⁻, and I⁻ solvated in water clusters, J. Chem. Phys. 101 (1994) 9344–9353.
[10] D. Liu, G. Ma, L.M. Levering, H.C. Allen, Vibrational spectroscopy of aqueous sodium halide solutions and air-liquid interfaces: Observation of increased interfacial depth, J. Phys. Chem. B 108 (2004) 2252–2260.
[11] P.B. Petersen, J.C. Johnson, K.P. Knutsen, R.J. Saykally, Direct experimental validation of the Jones-Ray effect, Chem. Phys. Letters 397 (2004) 46–50.
[12] V. Padmanabhan, J. Daillant, L. Belloni, S. Mora, M. Alba, O. Konovalov, Specific ion adsorption and short-range interactions at the air aqueous solution interface, Phys. Rev. Letters 99 (2007), 086105.
[13] L. Perera, M.L. Berkowitz, Many-body effects in molecular dynamics simulations of Na⁺(H₂O)ₙ and Cl⁻(H₂O)ₙ clusters, J. Chem. Phys. 95 (1991) 91954–91963.
[14] L.X. Dang, D.E. Smith, Molecular dynamics simulations of aqueous ionic clusters using polarizable water, J. Chem. Phys. 95 (1991) 6950–6956.
[15] L. Perera, M.L. Berkowitz, Structures of Cl⁻(H₂O)ₙ and F⁻(H₂O)ₙ (n=2,3,…,15) clusters. Molecular dynamics computer simulations, J. Chem. Phys. 100 (1994) 3085–3093.
[16] P. Jungwirth, D.J. Tobias, Molecular structure of salt solutions: A new view of the interface with implications for heterogeneous atmospheric chemistry, J. Phys. Chem. B. 105 (2001) 10468–10472.
[17] P. Jungwirth, D.J. Tobias, Ions at the air/water interface, J. Phys. Chem. B 106 (2002) 6361–6373.
[18] L. Vrbka, M. Mucha, B. Minofar, P. Jungwirth, E.C. Brown, D.J. Tobias, Propensity of soft ions for the air/water interface, Curr. Opin. Coll. Interface Sci. 9 (2004) 67–73.
[19] B.J. Eggimann, J.I. Siepmann, Size effects on the solvation of anions at the aqueous liquid-vapor interface, J. Phys. Chem. C 112 (2008) 201–218.
[20] D.J.V.A. dos Santos, F. Müller-Plathe, V.C. Weiss, Consistency of ion adsorption and excess surface tension in molecular dynamics simulations of aqueous salt solutions, J. Phys. Chem. C 112 (2008) 19431–19442.
[21] D. Horinek, A. Herz, L. Vrbka, F. Sedlmeier, S.I. Mamatkulov, R.R. Netz, Specific ion adsorption at the air/water interface: The role of hydrophobic solvation, Chem. Phys. Letters 479 (2009) 173–183.
[22] N. Ottosson, J. Heyda, E. Wernersson, W. Pokapanich, S. Svensson, B. Winter, G. Öhrwall, P. Jungwirth, O. Björneholm, The influence of concentration on the molecular surface structure of simple and mixed aqueous electrolytes, Phys. Chem. Chem. Phys. 12 (2010) 10693–10700.
[23] F. Bresme, E. Chacón, P. Tarazona, A. Wynveen, The structure of ionic aqueous solutions at interfaces: An intrinsic structure analysis, J. Chem. Phys. 137 (2012), 114706.
[24] A.C. Stern, M. Baer, C.J. Mundy, D.J. Tobias, Thermodynamics of iodine adsorption at the instantaneous air-water interface, J. Chem. Phys. 138 (2013), 114709.
[25] G. Olivieri, K.M. Parry, R. D'Auria, D.J. Tobias, M.A. Brown, Specific anion effects on Na⁺ adsorption at the aqueous solution–air interface: MD simulations, SESSA calculations, and photoelectron spectroscopy experiments, J. Phys. Chem. B 122 (2018) 910–918.
[26] J. Škvára, I. Nezbeda, Surface of aqueous solutions of alkali halides: Layer by layer analysis, Mol. Simul. 45 (2019) 358–372.
[27] C.V. Nguyen, H. Nakahara, O. Shibata, C.M. Phan, Adsorption of sodium iodine at the air/water interface, J. Mol. Liq. 298 (2020) 112076.
[28] G. Hantal, R.A. Horváth, J. Kolafa, M. Sega, P. Jedlovszky, Surface affinity of alkali and halide ions in their aqueous solution: Insight from intrinsic density analysis, J. Phys. Chem. B 124 (2020) 9884–9897.
[29] G. Hantal, J. Kolafa, M. Sega, P. Jedlovszky, Single particle dynamics at the intrinsic surface of aqueous alkali halide solutions, J. Phys. Chem. B 125 (2021) 665–679.
[30] M.D. Baer, C.J. Mundy, Toward an understanding of the specific ion effect using density functional theory, J. Phys. Chem. Letters 2 (2011) 1088–1093.
[31] Y. Levin, Polarizable ions at interfaces, Phys. Rev. Letters 102 (2009), 147803.
[32] Y. Levin, A.P. dos Santos, A. Diehl, Ions at the air-water interface: An end to a hundred-year-old mystery? Phys. Rev. Letters 103 (2009), 257802.
[33] M. Lbadaoui-Darvas, A. Idrissi, P. Jedlovszky, Computer simulation of the surface of aqueous ionic and surfactant solutions, J. Phys. Chem. B 126 (2022) 751–765.
[34] T. Seki, C.C. Yu, K.Y. Chiang, A. Greco, X. Yu, F. Matsumura, M. Bonn, Y. Nagata, Ion speciation at the water-air interface, J. Am. Chem. Soc. 145 (2023) 10622–10630.
[35] L. McFegan, Á. Juhász, P. Márton, Z. Hórvölgyi, A. Jedlovszky-Hajdu, G. Hantal, P. Jedlovszky, Surface affinity of tetramethylammonium iodide in aqueous solutions – a combined experimental and computer simulation study, J. Phys. Chem. B 127 (2023) 5341–5352.
[36] G. Hantal, M. Klíma, L. McFegan, J. Kolafa, P. Jedlovszky, Does the sign of charge affect the surface affinity of simple ions? J. Phys. Chem. B (in press).
[37] J.S. Rowlinson, B. Widom, Molecular theory of capillarity, Dover Publications, Mineola, 2002.
[38] E. Chacón, P. Tarazona, Intrinsic profiles beyond the capillary wave theory: A Monte Carlo study, Phys Rev. Letters 91 (2003), 166103.
[39] J. Chowdhary, B.M. Ladanyi, Water-Hydrocarbon Interfaces: Effect of hydrocarbon branching on interfacial structure, J. Phys. Chem. B. 110 (2006) 15442–15453.
[40] M. Jorge, M.N.D.S. Cordeiro, Intrinsic structure and dynamics of the water/nitrobenzene interface, J. Phys. Chem. C. 111 (2007) 17612–17626.
[41] L.B. Pártay, G. Hantal, P. Jedlovszky, Á. Vincze, G. Horvai, A new method for determining the interfacial molecules and characterizing the surface roughness in computer simulations. Application to the liquid–vapor interface of water, J. Comp. Chem. 29 (2008) 945–956.
[42] A.P. Wilard, D. Chandler, Instantaneous liquid interfaces, J. Phys. Chem. B. 114 (2010) 1954–1958.
[43] M. Sega, S. Kantorovich, P. Jedlovszky, M. Jorge, The generalized identification of truly interfacial molecules (ITIM) algorithm for nonplanar interfaces, J. Chem. Phys. 138 (2013), 044110.
[44] M. Jorge, P. Jedlovszky, M.N.D.S. Cordeiro, A critical assessment of methods for the intrinsic analysis of liquid interfaces. 1. Surface site distributions, J. Phys. Chem. C. 114 (2010) 11169–11179.
[45] M. Sega, B. Fábián, P. Jedlovszky, Layer-by-layer and intrinsic analysis of molecular and thermodynamic properties across soft interfaces, J. Chem. Phys. 143 (2015), 114709.
[46] L.B. Pártay, P. Jedlovszky, Á. Vincze, G. Horvai, Properties of Free Surface of Water-Methanol Mixtures. Analysis of the truly interfacial molecular layer in computer simulation, J. Phys. Chem. B. 112 (2008) 5428–5438.
[47] G. Hantal, M. Darvas, L.B. Pártay, G. Horvai, P. Jedlovszky, Molecular level properties of the free water surface and different organic liquid/water interfaces, as seen from ITIM analysis of computer simulation results, J. Phys.: Condens. Matter 22 (2010), 284112.
[48] M. Jorge, G.y. Hantal, P. Jedlovszky, M.N.D.S. Cordeiro, A critical assessment of methods for the intrinsic analysis of liquid interfaces. 2. Density profiles, J. Phys. Chem. C. 114 (2010) 18656.
[49] L.B. Pártay, P. Jedlovszky, Temperature and pressure dependence of the properties of the liquid-liquid interface. A computer simulation and identification of the truly interfacial molecules investigation of the water-benzene system, J. Phys. Chem. C. 114 (2010) 21681–21693.
[50] K.A. Perrine, K.M. Parry, A.C. Stern, M.H.C. Van Spyk, M.J. Makowski, J.A. Freites, B. Winter, D.J. Tobias, J.C. Hemminger, Specific cation effects at aqueous

solution−vapor interfaces: Surfactant-like behavior of Li$^+$ revealed by experiments and simulations, Proc. Natl. Acad. Sci. 114 (2017) 13363–13368.

[51] B. Fábián, G. Horvai, M. Sega, P. Jedlovszky, Single particle dynamics at the intrinsic surface of various apolar, aprotic dipolar, and hydrogen bonding liquids as seen from computer simulations, J. Phys. Chem. B 121 (2017) 5582–5594.

[52] E.J.W. Verwey, Theory of the stability of lyophobic colloids, J. Phys. Chem. 51 (1947) 631–636.

[53] P.T. Kiss, A. Baranyai, A new polarizable force field for alkali and halide ions, J. Chem. Phys. 141 (2014), 114501.

[54] P.T. Kiss, A. Baranyai, A systematic development of a polarizable potential of water, J. Chem. Phys. 138 (2013), 204507.

[55] J. Kolafa, MACSIMUS, release 2019-10-08 with blend V2.4a and cook V3.3k. Freely available software from URL: http://old.vscht.cz/fch/software/macsimus/ (last accessed: 23 May, 2023).

[56] M.P. Allen, D.J. Tildesley, Computer simulation of liquids, Clarendon Press, Oxford, 1987.

[57] P. Ewald, Die Berechnung optischer und elektrostatischer Gitterpotentiale, Ann. Phys. 369 (1921) 253–287.

[58] S.W. de Leeuw, J.W. Perram, E.R. Smith, Simulation of electrostatic systems in periodic boundary conditions. I. Lattice sums and dielectric constants, Proc. R. Soc. Lond. A 373 (1980) 27–56.

[59] I.C. Yeh, M.L. Berkowitz, Ewald summation for systems with slab geometry, J. Chem. Phys. 111 (1999) 3155–3162.

[60] J.P. Ryckaert, G. Ciccotti, H.J.C. Berendsen, Numerical integration of the Cartesian equations of motion of a system with constraints; molecular dynamics of n-alkanes, J. Comp. Phys. 23 (1977) 327–341.

[61] S. Nosé, A molecular dynamics method for simulations in the canonical ensemble, Mol. Phys. 52 (1984) 255–268.

[62] W.G. Hoover, Canonical dynamics: equilibrium phase-space distributions, Phys. Rev. A 31 (1985) 1695–1697.

[63] J. Kolafa, Time-reversible always stable predictor-corrector method for molecular dynamics of polarizable molecules, J. Comp. Chem. 25 (2004) 335–342.

[64] I.S. Joung, T.E. Cheatham III, Determination of alkali and halide monovalent ion parameters for use in explicitly solvated biomolecular simulations, J. Phys. Chem. B 112 (2008) 9020–9041.

[65] H.J.C. Berendsen, J.R. Grigera, T.P. Straatsma, The missing term in effective pair potentials, J. Phys. Chem. 91 (1987) 6269–6271.

[66] M.J. Abraham, T. Murtola, R. Schulz, S. Páll, J.C. Smith, B. Hess, E. Lindahl, GROMACS: High performance molecular simulations through multi-level parallelism from laptops to supercomputers, SoftwareX 1–2 (2015) 19–25.

[67] U. Essman, L. Perera, M.L. Berkowitz, T. Darden, H. Lee, L.G. Pedersen, A smooth particle mesh Ewald method, J. Chem. Phys. 103 (1995) 8577–8594.

[68] P. J. in't Veld, A. E. Ismail, G. S. Grest, Application of Ewald summations to long–range dispersion forces, J. Chem. Phys. 127 (2007) 144711.

[69] S. Miyamoto, P.A. Kollman, Settle: An analytical version of the SHAKE and RATTLE algorithm for rigid water models, J. Comp. Chem. 13 (1992) 952–962.

[70] URL: https://github.com/Marcello-Sega/pytim, (last accessed: 21 April, 2023).

[71] M. Sega, G. Hantal, B. Fábián, P. Jedlovszky, Pytim: A python package for the interfacial analysis of molecular simulations, J. Comp. Chem. 39 (2018) 2118–2125.

[72] C.Y. Lee, J.A. McCammon, P.J. Rossky, The structure of liquid water at an extended hydrophobic surface, J. Chem. Phys. 80 (1984) 4448–4455.

[73] V.P. Sokhan, D.J. Tildesley, The free surface of water: molecular orientation, surface potential and nonlinear susceptibility, Mol. Phys. 92 (1997) 625–640.

[74] P. Kiss, M. Darvas, A. Baranyai, P. Jedlovszky, Surface properties of the polarizable Baranyai-Kiss water model, J. Chem. Phys. 136 (2012) 114706.

[75] E.J. Verwey, J.T.G. Overbeek, Theory of the stability of lyophobic colloids, Elsevier, New York, 1948.

[76] R. Buchner, G.T. Hefter, P.M. May, Dielectric relaxation of aqueous NaCl solutions, J. Phys. Chem. A 103 (1999) 1–9.

[77] M. Sega, S. Kantorovich, A. Arnold, Kinetic dielectric decrement revisited: phenomenology of finite ion concentrations, Phys. Chem. Chem. Phys. 17 (2015) 130–133.